Materials Advances

ROYAL SOCIETY OF CHEMISTRY

PAPER

View Article Online
View Journal | View Issue

Cite this: *Mater. Adv.*, 2025, 6, 719

Carbon dot based fluorescent "on–off–on" assays for the determination of Au(III) ions and biothiols†

Zhenzhen Guo,[ac] Jinwen Zhu,[a] Yue Huang,[d] Jibin Liu*[b] and Peng Miao *[ac]

Received 18th October 2024,
Accepted 10th December 2024

DOI: 10.1039/d4ma01052c

rsc.li/materials-advances

Gold (Au) is extensively used in modern industry, which raises hard-to-ignore environmental problems due to its potential toxicity. Herein, highly luminescent carbon dots (CDs) are prepared from the carbon sources of *o*-phenylenediamine and hydroquinone, and applied for the selective quantification of Au^{3+}. Significantly, fluorescence quenching is observed upon the addition of Au^{3+} in 2 min. The ions are reduced to gold shells which coat the surface of CDs, resulting in electron transfer and emission quenching. The degree of quenching varies linearly with an Au^{3+}concentration from 0.1 to 7 μM. Biothiols are then introduced to interact with the gold shells. It is found that cysteine, glutathione, 3-mercaptopropionic acid and DL-dithiothreitol can be used to digest the shell, restoring the fluorescence emission. The "on–off–on" fluorescence biosensing strategy is challenged with environmental and biological samples with excellent results, demonstrating that this study provides a novel methodology to examine Au^{3+} and biothiol levels for potential practical applications.

Introduction

Macroscopic gold (Au) is widely used in modern industry (*e.g.*, in the manufacturing of jewelry and electronic products).[1] On the other hand, nanoscale Au is as an important element for synthetic chemistry,[2] analytical chemistry,[3] catalysis,[4] and biomedicine.[5] For example, Beqa *et al.* fabricated glutathione (GSH) modified Au nanoparticles (AuNPs) as dynamic light scattering (DLS) probes for colorimetric analysis of Pb(II) ions.[6] Kim *et al.* developed a cadaverine gas sensor with graphene-encased Au nanorods (AuNRs), which exhibited an ultrasensitive peak wavelength shift even with tiny molecules.[7] Although Au based nanomaterials have demonstrated to be chemically inert and possess high biocompatibility, ionic Au^{3+} has deleterious effects on the environment and human health.[8] Au^{3+} is able to interact with DNA and proteins, disrupting a series of cellular processes. Due to the food chain enrichment effect, Au^{3+} with high concentration may exhibit toxicity toward the liver, kidney and peripheral nervous system of human beings.[9] Therefore, it is necessary to develop highly reliable methods for the determination of Au^{3+}.[10] Traditional methods for Au^{3+} assay include inductively-coupled plasma mass spectroscopy (ICP-MS),[11] atomic absorption spectroscopy emission spectroscopy (AAS/AES),[12] and flame atomic absorption spectroscopy (FAAS).[13] However, these techniques require complicated sample preparation procedures, sophisticated instruments or time-consuming reactions.

Biothiols like cysteine (Cys) and GSH are ubiquitous in biological systems, playing important roles in human physiology.[14,15] Abnormal expressions of biothiols are always directly associated with diseases, including liver damage, leucocyte loss, psoriasis, edema, Alzheimer's disease, and so on. Using a fluorescent biosensor is an efficient methodology for the analysis of ions and biomolecules due to the merits of simplicity, high sensitivity and selectivity.[16–19] Over the past decade, a number of fluorescent probes have been reported for assays of Au^{3+} and biothiols.[20–23] However, most of the previously reported fluorescent probes were amended with recognition motifs by organic fluorophores such as rhodamine, coumarin, naphthalimide, and fluorescein. The photostabilities are always limited. Therefore, novel probes with improved optical properties are desired to tackle these problems. Carbon dots (CDs), as a new class of carbon-based nanomaterials, have received extensive attention in various fields especially in sensing, imaging, drug delivery and photocatalysis.[24–26] CDs exhibit outstanding fluorescence properties and merits including convenient preparation, easy functionalization, and good chemical stability.[27–29] The functional groups on the surface of CDs (*e.g.*, amino, hydroxyl, carbonyl, and carboxyl group) enhance the water solubility and promote surface modification.[30] Therefore, CDs have demonstrated to be good fluorescent probes for environmental and biological applications. On the other hand,

[a] *Suzhou Institute of Biomedical Engineering and Technology, Chinese Academy of Sciences, Suzhou 215163, China. E-mail: miaopeng@sibet.ac.cn*
[b] *Institute of Oncology, Affiliated Tumor Hospital of Nantong University, Nantong 226361, China. E-mail: tians2008@ntu.edu.cn*
[c] *Shandong Laboratory of Advanced Biomaterials and Medical Devices in Weihai, Weihai 264200, China*
[d] *Department of Food Science and Engineering, College of Light Industry and Food Engineering, Nanjing Forestry University, Nanjing 210037, China*

† Electronic supplementary information (ESI) available: Fig. S1–S7 and Table S1. See DOI: https://doi.org/10.1039/d4ma01052c

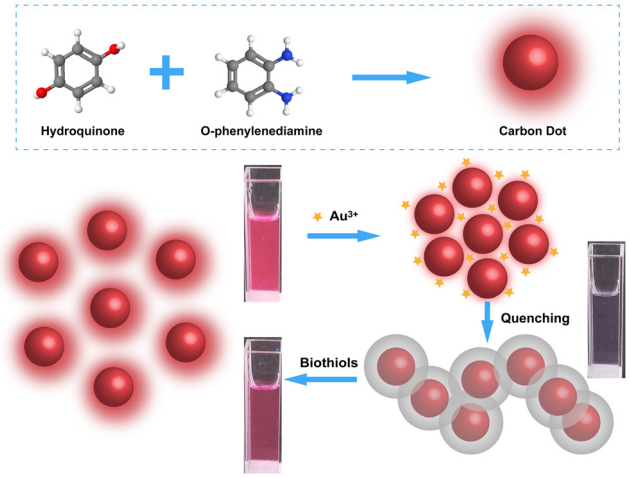

Scheme 1 Illustration of CD preparation and the sensing principle.

the design of nanohybrids incorporating CDs and other nanomaterials may extend their range of applications.[31–34]

In this contribution, we synthesize red-emissive CDs through a one-step solvothermal method and fabricate sensitive "on–off–on" assays of Au^{3+} and biothiols. The working principle is shown in Scheme 1. Hydroquinone and *o*-phenylenediamine are chosen as the carbon sources. After the addition of Au^{3+}, electrostatic repulsion between particles is weakened and the dots are brought together. Nitrogen-containing functional groups on the surface of CDs have high reduction abilities, leading to the transformation of Au^{3+} into Au(0). Gold shells can thus be formed around CDs, leading to the electron transfer and fluorescence quenching phenomenon. By measuring the remarkable decline of fluorescence emission, the concentration of Au^{3+} can be determined. On the other hand, biothiols like Cys and GSH can be used to digest the shells and restore the fluorescence. The "on–off–on" fluorescent biosensors have good prospects in both environmental monitoring and medical diagnosis.

Experimental

Materials and chemicals

Chloroauric acid ($HAuCl_4 \cdot 3H_2O$), *o*-phenylenediamine, hydroquinone, sulfuric acid (H_2SO_4), ammonium persulphate (AP), DL-dithiothreitol (DTT), 3-morpholinopropane sulfonic acid (MOPS), ammonium hydroxide, ethanol, lithium chloride (LiCl), sodium chloride (NaCl), potassium chloride (KCl), silver nitrate ($AgNO_3$), copper nitrate ($Cu(NO_3)_2$), zinc chloride ($ZnCl_2$), cadmium chloride ($CdCl_2$), calcium chloride ($CaCl_2$), magnesium chloride ($MgCl_2$), manganese chloride ($MnCl_2$), aluminum chloride ($AlCl_3$), nickel chloride ($NiCl_2$), mercury nitrate ($Hg(NO_3)_2$), lead nitrate ($Pb(NO_3)_2$), iron(II) chloride ($FeCl_2$), and iron(III) chloride ($FeCl_3$) were purchased from Sigma-Aldrich (USA). GSH, Cys, homocysteine (Hcy), alanine (Ala), arginine (Arg), glycine (Gly), histidine (His), proline (Pro), lysine (Lys), serine (Ser), tryptophan (Trp), valine (Val), aspartic acid (Asp), methionine (Met), glutamic acid (Glu), phenylalanine (Phe), tyrosine (Tyr), 3-mercaptopropionic acid (3-MPA), ascorbic acid, glucose, and sodium sulfide nonahydrate were purchased from Shanghai Macklin Biochemical Technology Co., Ltd. (Shanghai, China). Serum samples were collected from Affiliated Tumor Hospital of Nantong University. All other reagents were of analytical grade and used without further purification. Water used to prepare solutions was purified with a Millipore system (18.2 MΩ cm, 25 °C).

Instruments

Transmission electron microscopy (TEM) images were taken using an FEI Tecnai G20 transmission electron microscope (FEI, USA). Fourier transform infrared (FTIR) spectra were measured using an Agilent Cary 660 FTIR spectrometer (Agilent Technologies, USA). UV-vis absorption spectra were recorded using a NanoDrop OneC spectrophotometer (Thermo Scientific, USA). X-ray photoelectron spectra (XPS) were recorded using an AXIS UltraDLD X-ray photoelectron spectrometer (Kratos, Japan). Fluorescence excitation and emission spectra were measured using a Hitachi F-4600 fluorescence spectrophotometer (Hitachi, Japan). Quantum yield was determined using an FLS1000 photoluminescence spectrometer (Edinburgh Instruments, UK).

Preparation of CDs

216 mg of *o*-phenylenediamine and 220 mg of hydroquinone were dissolved in 10 mL of deionized water. 1 mL of sulfuric acid was then added, followed by ultrasonicating for 10 min. The mixture was transferred to a poly(tetrafluoroethylene) (Teflon)-lined autoclave (25 mL), which was heated at 180 °C for 10 h. Afterward, the solution was cooled down to room temperature slowly. Ammonium hydroxide was then added to achieve neutral conditions. A dark red solid was precipitated, which was washed with water three times and dried under vacuum at 60 °C.

Fluorescence quantification of Au^{3+} and sulfhydryl compounds

Standard Au^{3+} solutions were prepared with a series of concentrations. CD was dissolved in 0.02 M PBS (pH = 7.4) and ethanol (1 : 1) with a concentration of 17 μg mL^{-1}. 5 μL of Au^{3+} was spiked in 995 μL of CD. After reacting for 2 min, fluorescence spectra were measured at an excitation wavelength of 540 nm. To achieve the analysis of Cys and GSH, CD/Au^{3+} solutions were prepared with concentrations of 17 μg mL^{-1} and 6 μM, respectively. Then, 5 μL of Cys or GSH was added to the above solutions. After reacting for 15 min, fluorescence spectra were measured.

Real sample assays

Lake water samples were collected and filtered using filtration membranes (0.22 μm). Afterward, 100 μL of the samples and 400 μL of 0.02 M PBS (pH = 7.4) were mixed with 500 μL of CD solution (34 μg mL^{-1}). The mixtures were stirred before the addition of Au^{3+}. After that, fluorescence emission spectra were recorded for the analysis of Au^{3+}. For the detection of Cys and GSH in serum samples, the mixtures of serum and CD/Au^{3+} were first prepared with the volume ratio of 10 μL : 990 μL. The following operations were similar to the above ones.

Results and discussion

Characterization of CDs

The morphology of the CDs was first characterized by TEM. As shown in Fig. 1A, the shape of the CDs is quasi-spherical and the dispersibility is excellent. The diameter of the CDs ranges between 1.77 and 8.40 nm, with an average size of 3.90 nm. From the EDS analysis, the major element is found to be carbon with a ratio over 90% (Fig. 1B). To probe the functional groups of CDs, an FTIR spectrum is recorded. As shown in Fig. 1C, the broad absorption peak around 3245 cm^{-1} belongs to the stretching vibration of O–H or N–H. The peak at 3035 cm^{-1} is ascribed to the stretching vibrations of C–H. The 1581 cm^{-1} and 1476 cm^{-1} peaks are from the C═C vibrations on the benzene ring. The 1219 cm^{-1} and 1096 cm^{-1} peaks are from C═S and C–O/C–N, respectively. In addition, the peaks at 808 cm^{-1}, 752 cm^{-1}, and 730 cm^{-1} are ascribed to the bending vibrations of C–H. After interaction between the CDs and Au^{3+}, the intensities of the N–H stretching and C–N stretching bands are weakened, suggesting the reaction occurs between amino groups and Au^{3+}. Next, the composition of CD is characterized by XPS. The scanning spectra indicate the CDs contain C, N, O and S elements. The characteristic peaks of C 1s, N 1s, O 1s and S 2p are 284.80 eV, 399.83 eV, 531.9 eV and 163.94 eV, respectively (Fig. S1A, ESI†). The high-resolution spectra of C 1s, N 1s O 1s and S 2p are also recorded, respectively. For C 1s, the peaks of 284.50 eV, 285.05 eV, and 288.65 eV are for C–C/C═C, C–N(O,S), and C═O (Fig. S1B, ESI†); for N 1s, the peaks at 398.5 eV, 399.9 eV and 400.99 eV indicate the presence of C–N, C–N–C and N–H bonds (Fig. S1C, ESI†); for O 1s, the peaks at 531.8 eV and 533.0 eV correspond to C–O and C–O–H bonds (Fig. S1D, ESI†); for S 2p, three peaks at 163.8 eV, 164.8 eV and 168.7 eV suggest the presence of S 2p2/3 C–S–C, S 2p1/2 C–S–C, and C–SO_x, respectively (Fig. S1E, ESI†). The results of XPS and FTIR are quite consistent, demonstrating that CDs are rich in various functional groups, such as amino, hydroxyl and carbonyl groups on their surfaces. After interaction with Au^{3+}, thick gold layers are deposited on the surface of the CDs, which can be clearly observed in the TEM image (Fig. 1D). The formed layer is more visible compared with the CDs. In the XPS high-resolution survey scan of Au element (Fig. S1F, ESI†), two distinct characteristic peaks (84.78 eV and 88.38 eV) are obtained, which are assigned to the 4f7/2 and 4f5/2 features of Au(0). The presence of the elements of Au, C, O, N, and Cl is also evidenced by TEM-mapping (Fig. S2, ESI†). In addition, from the EDS analysis, the elemental ratio of Au is increased to about 30% (Fig. 1E). A Raman spectrum of the CDs was then recorded (Fig. S3, ESI†). Vibration peaks at 1384 and 1555 cm^{-1} are ascribed to the structures of sp^3 (D) and sp^2 (G), which indicate the graphitic structure of the CDs. The UV-vis absorption spectra of the CDs before and after interaction with Au^{3+} are compared in Fig. 1F. An obvious absorption around 540 nm appears for the CDs. After the addition of Au^{3+}, the absorption peak disappears, which may due to the formation of a gold layer. However, after further introduction of Cys, the peak can be restored, demonstrating the elimination of the gold layer. The zeta potential of bare CDs is measured to be −5.46 mV. After being coated with a gold layer, the zeta potential decreases to −12.3 mV, which is due to $[AuCl_4]^-$ ions outside the layer. After further treatment with Cys, the gold layer can be digested, exposing the CDs' core. Meanwhile, the zeta potential is measured to be less negative (−10.2 mV).

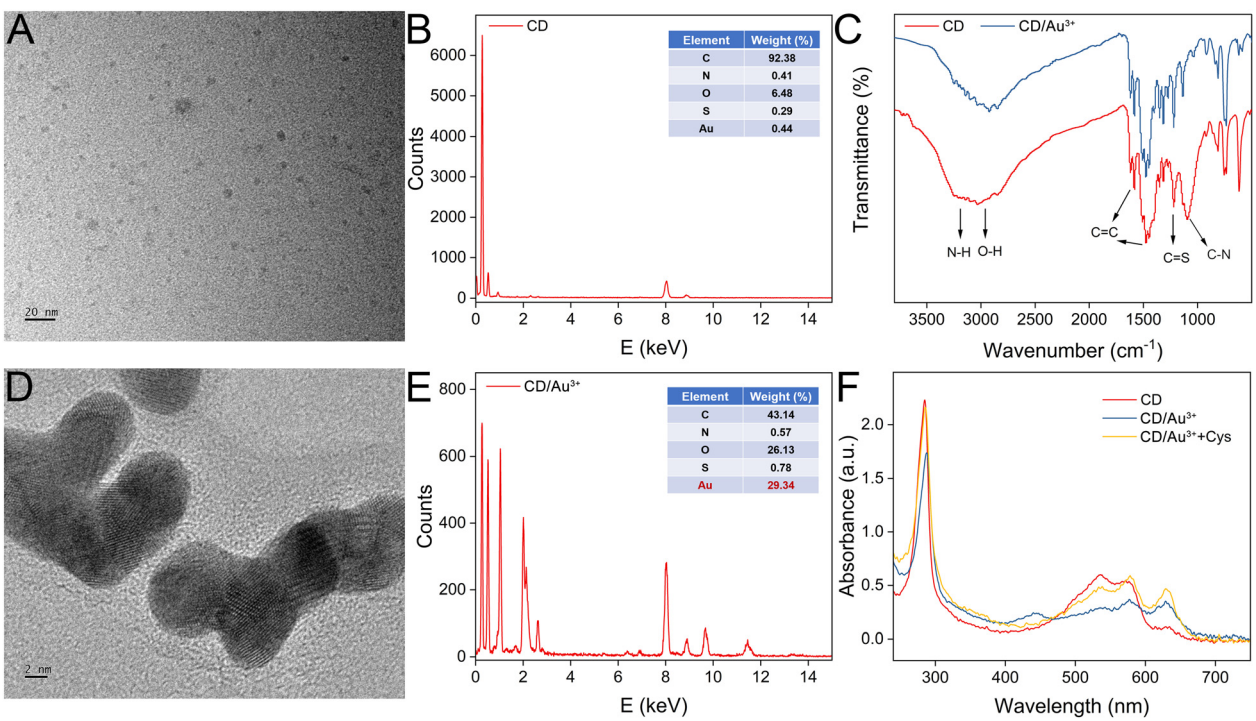

Fig. 1 (A) TEM image and (B) EDS spectrum of the CDs. (C) FTIR spectra of the CDs before and after reacting with Au^{3+}. (D) TEM image and (E) EDS spectrum of the CDs after reacting with Au^{3+}. (F) UV-vis absorption spectra of the CDs before and after reacting with Au^{3+} and Cys.

Fluorescence features of CDs

The fluorescence properties of CDs are carefully studied. The excitation and emission spectra are shown in Fig. 2A. The maximum excitation wavelength is 540 nm. After being excited with a series of wavelengths (from 340 to 560 nm), no significant shift of the emission peak (at 610 nm) can be observed, indicating the CDs have uniform size and surface states (Fig. 2B). The excitation wavelength of 540 nm which contributes to the largest emission, was then selected for the following fluorescence experiments (Fig. 2C). The value coincides with the absorption peak in the UV-vis spectra. The quantum yield of CDs is determined to be 46.79%, which is quite high (Fig. S4, ESI†). The stability of the CDs is then evaluated. As shown in Fig. 2D, the emission intensity shows scarce variation under UV light for a long time. In addition, the CDs show negligible fluorescence emission alterations (Fig. S5A and B, ESI†), challenging the circumstance of various salt concentrations (0 to 1 M) or temperatures (4 to 70 °C). We have also prepared CD solutions with different concentrations. The fluorescence emission spectra are overlaid (Fig. S5C, ESI†). The peak intensity first increases dramatically with larger concentration and reaches saturation. With further increase in concentration, it drops slightly. The optimized concentration of 17 μg mL^{-1} was chosen for the following experiments (Fig. S5D, ESI†).

The fluorescence quenching and recovery can be used for the analysis of Au^{3+} and biothiols. As shown in Fig. 2E, after blending CD and Au^{3+}, the fluorescence peak intensity drops significantly. Seven types of molecules (3-MPA, Cys, GSH, DTT, Hcy, AP and MOPS) are then introduced into the CD/Au^{3+} system. The peak intensities can only be restored by the first four molecules (Fig. 2F). The reason is that 3-MPA, Cys, GSH and DTT contain free thiol groups, which interact with gold layers effectively to eliminate the quenching effect. In contrast, Hcy commonly exists in the form of disulfide. AP and MOPS do not contain any thiol groups. Thus, the fluorescence emission cannot be restored. These results demonstrate the feasibility of "on–off–on" sensing of Au^{3+} and biothiols.

Experimental optimization and quantification of Au^{3+}

To achieve the best analytical performances, some critical parameters are first optimized by comparing the fluorescence intensities. After Au^{3+} addition, the peak intensity decreases with longer incubation time and becomes stable in 2 min (Fig. S6A, ESI†). After further introduction of Cys and GSH as examples of biothiols, the fluorescence peak intensities recover with longer incubation times, which are basically unchanged in 15 min (Fig. S6B and C, ESI†). Therefore, the optimized reaction times are set for the following experiments. We then prepared standard Au^{3+} solutions with concentrations from 0.1 to 10 μM. Fig. 3A displays the fluorescence spectra of CDs after reaction with Au^{3+} for 2 min. The peak intensity decreases progressively with the level of Au^{3+}. We then obtained the relationship between the concentration of Au^{3+} and the fluorescence peak, which is shown in Fig. 3B. The inset reflects the linear range from 0.1 to 7 μM. The equation is fitted as follows:

$$y = 6183.15 - 874.95x \quad (R^2 = 0.998,\ n = 3)$$

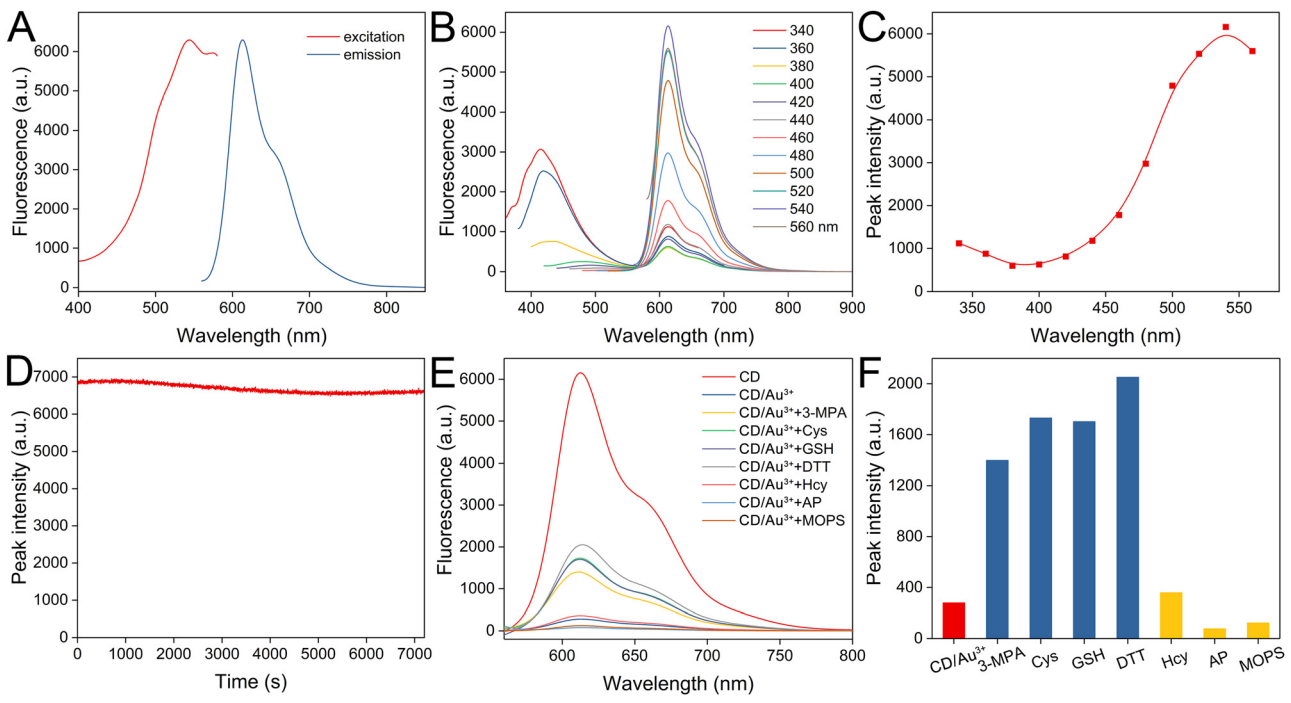

Fig. 2 (A) Fluorescence excitation and emission spectra of CDs. (B) Fluorescence emission spectra of CDs with different excitation wavelengths. (C) The relationship between the excitation wavelength and the fluorescence peak intensity (610 nm). (D) Fluorescence stability of CDs. (E) Fluorescence emission spectra of CDs, CD/Au^{3+}, CD/Au^{3+} + 3-MPA, CD/Au^{3+} + Cys, CD/Au^{3+} + GSH, CD/Au^{3+} + DTT, CD/Au^{3+} + Hcy, CD/Au^{3+} + AP, and CD/Au^{3+} + MOPS. (F) The corresponding peak fluorescence intensities.

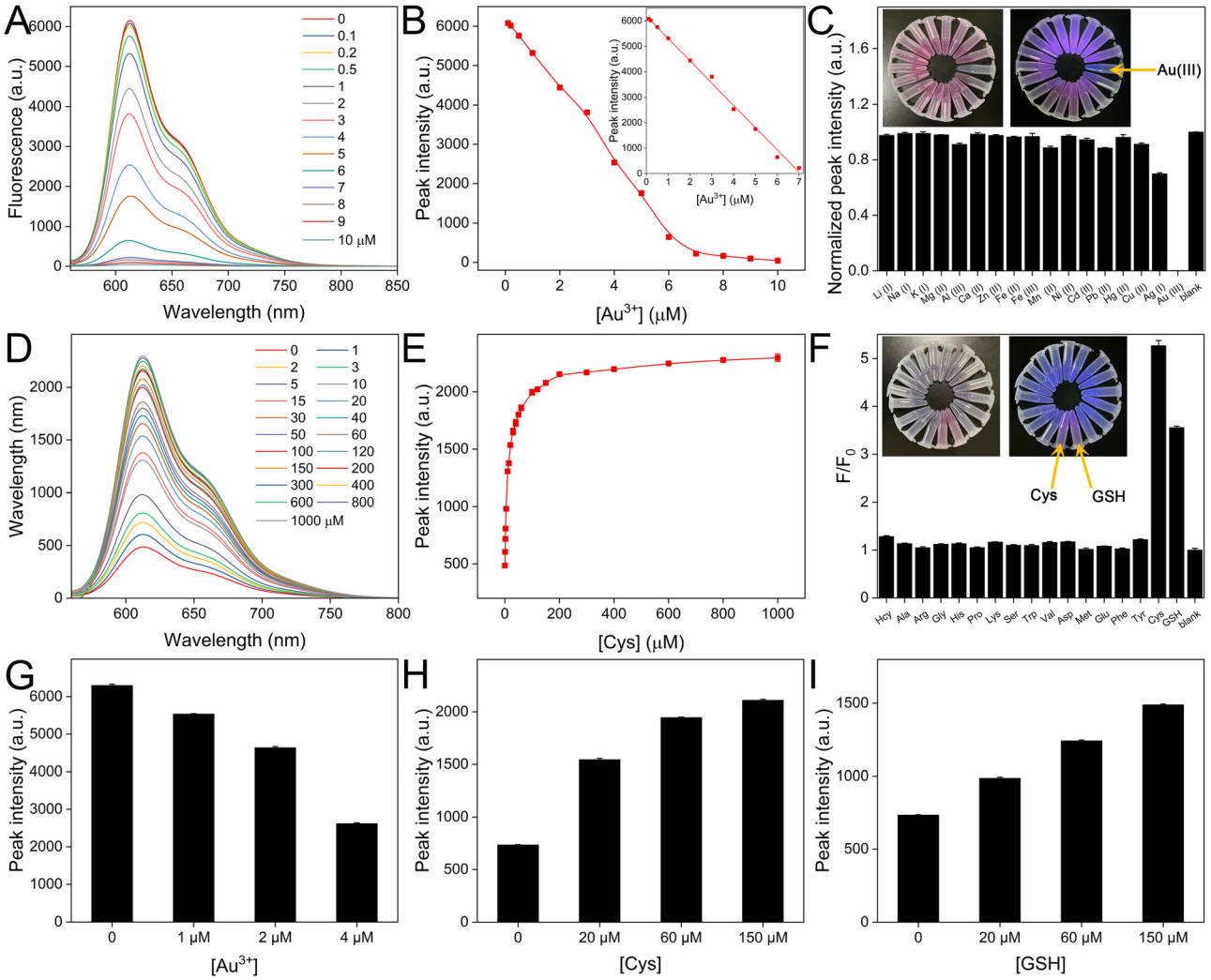

Fig. 3 (A) Fluorescence spectra for the detection of Au^{3+} with a series of concentrations. (B) The relationship between the concentration of Au^{3+} and the peak intensity. The inset shows the linear range. (C) Fluorescence peak intensities of CDs after blending with different types of ions. The inset shows the pictures excited by daylight (left) and using a 365 nm UV lamp (right). (D) Fluorescence spectra for the detection of Cys with a series of concentrations. (E) The relationship between the concentration of Cys and the peak intensity. (F) Fluorescence peak intensities of CD/Au^{3+} after blending with different types of amino acids and GSH. The inset shows the pictures excited by daylight (left) and using a 365 nm UV lamp (right). Fluorescence response of CDs in real samples spiked with different concentrations of (G) Au^{3+}, (H) Cys, and (I) GSH.

in which y is the fluorescence peak intensity, and x represents the concentration of Au^{3+} (μM). The limit of detection is calculated to be 10 nM (S/N = 3), which shows certain superiority compared with most recently reported biosensors (Table S1, ESI†). To demonstrate the selectivity of CDs towards Au^{3+}, we tested 16 different common metal ions as potential interfering substances. The concentration of Au^{3+} is 10 μM, while the concentration of other ions is 100 μM. The obtained peak intensities are listed in Fig. 3C. The fluorescence intensities are not significantly affected by the interfering substances even with 10 times higher concentrations. The reason is that our prepared CDs exhibit weak binding capabilities with these ions and cannot reduce them like Au^{3+}.

Quantification of biothiols based on CD-Au^{3+}

The fluorescence of CDs quenched by Au^{3+} can be restored by certain biothiols. The quantitative analysis is then studied. Fig. 3D illustrates the fluorescence spectra of the CD/Au^{3+} system after further reaction with Cys for 15 min. The peak intensity increases with a larger concentration of Cys and the detailed relationship is summarized in Fig. 3E. The recovery reaches saturation in 200 μM. Similar fluorescence recovery and quantitative analysis of GSH from 1 to 1000 μM are also achieved (Fig. S7, ESI†). We then introduced common amino acids as potential interfering molecules to study the selectivity of the CD/Au^{3+} system. The concentrations of Cys and GSH are 40 μM, while the other substances have concentrations of 400 μM. The fluorescence responses are listed in Fig. 3F. Cys and GSH can obviously restore the fluorescence. However, after treating with the other amino acids, the fluorescence intensities are nearly the same as the blank case. These results demonstrate the high selectivity of these ''on–off–on'' fluorescence biosensors.

Analysis of Au^{3+} and biothiols in real samples

To ensure the reliability of Au^{3+} analysis, lake water samples are employed and a standard addition method is performed. After spiking with different amounts of Au^{3+} in filtered lake water samples, the prepared CD solutions are mixed and the fluorescence emission spectra are recorded. With a larger concentration of spiked Au^{3+}, the peak intensity is smaller. After referring to the established equation for standard Au^{3+}, the concentrations of Au^{3+} in the lake samples are calculated, which approximate to the added concentrations (Fig. 3G). We have also collected serum samples. After diluting with PBS containing CD/Au^{3+}, the solutions were spiked with different concentrations of Cys and GSH. The increased fluorescence recovery can be observed with more biothiols (Fig. 3H and I), demonstrating that the biological samples do not significantly interfere with the sensing system. This demonstrates that the proposed "on–off–on" biosensor shows great potential for practical applications.

Conclusions

In summary, we have achieved the synthesis of bright CDs through a one-pot solvothermal method. *o*-Phenylenediamine and hydroquinone are selected as the carbon precursors. The prepared CDs exhibit satisfactory photostability, high sensitivity and selectivity towards Au^{3+} sensing. After the ions are reduced to Au(0), the fluorescence emission of the CDs is effectively quenched due to the electron transfer. The decline in intensity reflects the level of initial Au^{3+}. Moreover, biothiols including Cys and GSH preferentially interact with the gold layers around the CDs, leading to the recovery of fluorescence emission, realizing "on–off–on" sensing performances. The analytical results of Au^{3+} and biothiols in real samples also indicate good performances. In general, the proposed strategy has promising prospects in environmental and biological fields.

Author contributions

Zhenzhen Guo: conceptualization, investigation, and writing – original draft. Jinwen Zhu: investigation and formal analysis. Yue Huang: investigation and validation. Jibin Liu: validation and writing – review & editing. Peng Miao: conceptualization, validation, writing – review & editing, and supervision.

Data availability

The data supporting this article have been included as part of the ESI.†

Conflicts of interest

There are no conflicts to declare.

Acknowledgements

This work is supported by the National Key Research and Development Program of China (2022YFC2403403) and the Project of Shandong Provincial Laboratory (SYS202207).

Notes and references

1 H. Shang, Y. Chen, S. Guan, Y. Wang, J. Cao, X. Wang, H. Li and Z. Bian, Scalable and selective gold recovery from end-of-life electronics, *Nat. Chem. Eng.*, 2024, **1**, 170–179.
2 S. Kashiwaya, Y. Shi, J. Lu, D. G. Sangiovanni, G. Greczynski, M. Magnuson, M. Andersson, J. Rosen and L. Hultman, Synthesis of goldene comprising single-atom layer gold, *Nat. Synth.*, 2024, **3**, 744–751.
3 Y. Li, P. Zhou, Z. Wang, Y. Ren, X. Zhu, J. Wang, H. Yan, L. Hua and F. Gao, Sea anemone-like nanomachine based on DNA strand displacement composed of three boolean logic gates: diversified input for intracellular multitarget detection, *Anal. Chem.*, 2024, **96**, 4120–4128.
4 Q. Wang, K. Sang, C. Liu, Z. Zhang, W. Chen, T. Ji, L. Li, C. Lian, G. Qian, J. Zhang, X. Zhou, W. Yuan and X. Duan, Nanoparticles as an antidote for poisoned gold single-atom catalysts in sustainable propylene epoxidation, *Nat. Commun.*, 2024, **15**, 3249.
5 H. S. Han, K. Y. Choi, H. Lee, M. Lee, J. Y. An, S. Shin, S. Kwon, D. S. Lee and J. H. Park, Gold-nanoclustered hyaluronan nano-assemblies for photothermally maneuvered photodynamic tumor Ablation, *ACS Nano*, 2016, **10**, 10858–10868.
6 L. Beqa, A. K. Singh, S. A. Khan, D. Senapati, S. R. Arumugam and P. C. Ray, Gold nanoparticle-based simple colorimetric and ultrasensitive dynamic light scattering assay for the selective detection of Pb(II) from paints, plastics, and water samples, *ACS Appl. Mater. Interfaces*, 2011, **3**, 668–673.
7 K. H. Kim, S. Jo, S. E. Seo, J. Kim, D.-S. Lee, S. Joo, J. Lee, H. S. Song, H. G. Lee and O. S. Kwon, Ultrasensitive gas detection based on electrically enhanced nanoplasmonic sensor with graphene-encased gold nanorod, *ACS Sens.*, 2023, **8**, 2169–2178.
8 C. Wang, G. Lin, J. Zhao, S. Wang, L. Zhang, Y. Xi, X. Li and Y. Ying, Highly selective recovery of Au(III) from wastewater by thioctic acid modified Zr-MOF: Experiment and DFT calculation, *Chem. Eng. J.*, 2020, **380**, 122511.
9 S.-H. Nam, W.-M. Lee, Y.-J. Shin, S.-J. Yoon, S. W. Kim, J. I. Kwak and Y.-J. An, Derivation of guideline values for gold (III) ion toxicity limits to protect aquatic ecosystems, *Water Res.*, 2014, **48**, 126–136.
10 V. Sharma, N. Kaur, P. Tiwari, A. K. Saini and S. M. Mobin, Multifunctional fluorescent "Off-On-Off" nanosensor for Au^{3+} and S^{2-} employing N-S co-doped carbon–dots, *Carbon*, 2018, **139**, 393–403.
11 M. V. B. Krishna, M. Ranjit, K. Chandrasekaran, G. Venkateswarlu and D. Karunasagar, On-line preconcentration and recovery of palladium from waters using polyaniline (PANI) loaded in mini-column and determination by ICP-MS; elimination of spectral interferences, *Talanta*, 2009, **79**, 1454–1463.
12 M. A. Janusa and J. N. Beck, Recent applications of flame atomic absorption spectrometry to environmental measurements, *Appl. Spectrosc. Rev.*, 2002, **37**, 137–186.

13 Y. Luo, B. Zhang, M. Chen, J. Wang, X. Zhang, W.-Y. Gao, J.-F. Huang and W.-L. Fu, Rapid and simultaneous determination of essential minerals and trace elements in human milk by improved flame atomic absorption spectroscopy (FAAS) with microwave Digestion, *J. Agric. Food Chem.*, 2010, **58**, 9396–9400.
14 R. Sharma, U. Haldar and H.-I. Lee, Two-in-one dual-channel boronic ester block copolymer for the colorimetric detection of cysteine and glucose at neutral pH, *ACS Sustainable Chem. Eng.*, 2021, **9**, 9915–9922.
15 X. Cheng, H.-D. Xu, H.-H. Ran, G. Liang and F.-G. Wu, Glutathione-depleting nanomedicines for synergistic cancer therapy, *ACS Nano*, 2021, **15**, 8039–8068.
16 A. Amalraj and P. Perumal, Label-free DNAzyme for highly sensitive detection of multiple biomolecules in real samples through target-triggered catalytic cleavage reactions with auramine O's discriminated fluorescence emission, *Anal. Bioanal. Chem.*, 2022, **414**, 4021–4037.
17 A. Ravikumar, P. Panneerselvam and N. Morad, Metal–polydopamine framework as an effective fluorescent quencher for highly sensitive detection of Hg(II) and Ag(I) ions through exonuclease III activity, *ACS Appl. Mater. Interfaces*, 2018, **10**, 20550–20558.
18 A. Amalraj, R. Pavadai and P. Perumal, Recyclable target metal-enhanced fluorometric naked eye aptasensor for the detection of Pb^{2+} and Ag^{+} ions based on the structural change of CaSnO3@PDANS-constrained GC-rich ssDNA, *ACS Omega*, 2021, **6**, 30580–30597.
19 A. Amalraj and P. Perumal, Dual fluorometric biosensor based on a nanoceria encapsulated metal organic framework and a signal amplification strategy of a hybridization chain reaction for the detection of melamine and Pb^{2+} ions in food samples, *New J. Chem.*, 2022, **46**, 12952–12967.
20 Y. Yang, B. Bai, M. Jin, Z. Xu, J. Zhang, W. Li, W. Xu, X. Wang and C. Yin, Fluorescent imaging of Au^{3+} in living cells with two new high selective Au^{3+} probes, *Biosens. Bioelectron.*, 2016, **86**, 939–943.
21 W. Gao, H. Song, X. Wang, X. Liu, X. Pang, Y. Zhou, B. Gao and X. Peng, Carbon dots with red emission for sensing of Pt^{2+}, Au^{3+}, and Pd^{2+} and their bioapplications *in vitro* and *in vivo*, *ACS Appl. Mater. Interfaces*, 2018, **10**, 1147–1154.
22 C. Xie, Y. Lyu, X. Zhen, Q. Miao and K. Pu, Activatable semiconducting oligomer amphiphile for near-infrared luminescence imaging of biothiols, *ACS Appl. Bio Mater.*, 2018, **1**, 1147–1153.
23 J. O. Lee, Y.-M. Yang, J.-H. Choi, T.-W. Kim, J.-W. Lee and Y.-P. Kim, Microbial redox regulator-enabled pulldown for rapid analysis of plasma low-molecular-weight biothiols, *Anal. Chem.*, 2019, **91**, 10064–10072.
24 X. Zhang, Y. Zhang, Y. Wang, S. Kalytchuk, S. V. Kershaw, Y. Wang, P. Wang, T. Zhang, Y. Zhao, H. Zhang, T. Cui, Y. Wang, J. Zhao, W. W. Yu and A. L. Rogach, Color-switchable electroluminescence of carbon dot light-emitting diodes, *ACS Nano*, 2013, **7**, 11234–11241.
25 S. Bhattacharya, R. S. Phatake, S. Nabha Barnea, N. Zerby, J.-J. Zhu, R. Shikler, N. G. Lemcoff and R. Jelinek, Fluorescent self-healing carbon dot/polymer gels, *ACS Nano*, 2019, **13**, 1433–1442.
26 S. Majumdar, G. Krishnatreya, N. Gogoi, D. Thakur and D. Chowdhury, Carbon-dot-coated alginate beads as a smart stimuli-responsive drug delivery system, *ACS Appl. Mater. Interfaces*, 2016, **8**, 34179–34184.
27 C. Wang, H. Lin, Z. Xu, Y. Huang, M. G. Humphrey and C. Zhang, Tunable Carbon-dot-based dual-emission fluorescent nanohybrids for ratiometric optical thermometry in living cells, *ACS Appl. Mater. Interfaces*, 2016, **8**, 6621–6628.
28 V. A. Ansi, P. Sreelakshmi, P. Raveendran and N. K. Renuka, Table sugar derived carbon dot—A promising green reducing agent, *Mater. Res. Bull.*, 2021, **139**, 111284.
29 Y. Zhu, J. Du, Q. Q. Peng, F. Y. Wang, J. Hu, Y. S. Luo, A. A. Alshehri, K. A. Alzahrani, B. Z. Zheng, X. P. Sun and D. Xiao, The synthesis of highly active carbon dot-coated gold nanoparticles via the room-temperature in situ carbonization of organic ligands for 4-nitrophenol reduction, *RSC Adv.*, 2020, **10**, 19419–19424.
30 G. Liu, H. Chai, Y. Tang and P. Miao, Bright carbon nanodots for miRNA diagnostics coupled with concatenated hybridization chain reaction, *Chem. Commun.*, 2020, **56**, 1175–1178.
31 S. Pawar, H. Duadi, Y. Fleger and D. Fixler, Design and use of a gold nanoparticle–carbon dot hybrid for a FLIM-based IMPLICATION nano logic gate, *ACS Omega*, 2022, **7**, 22818–22824.
32 Z. Z. Lu, L. W. Giles, B. M. Teo and R. F. Tabor, Carbon dots as a 'green' reagent to produce shape and size controlled gold nanoparticles for application in pollutant degradation, *Colloid Interface Sci. Commun.*, 2022, **46**, 100571.
33 S. Ghosh, S. S. Satapathy, K. Ghosh, S. Jauhari, S. K. Panda and S. Si, Carbon dots assisted synthesis of gold nanoparticles and their catalytic activity in 4-nitrophenol reduction, *ChemistrySelect*, 2019, **4**, 3416–3422.
34 P. Suresh Kumar, S. Megarajan, G. Rajendra Kumar Reddy and V. Anbazhagan, Facile synthesis of gold nanoparticles using carbon dots for electrochemical detection of neurotransmitter, dopamine in human serum and as a chemocatalyst for nitroaromatic reduction, *IET Nanobiotechnol.*, 2018, **12**, 909–914.